Growth and Alignment of Thin Film Organic Single Crystals from Dewetting Patterns

Jean-Nicolas Tisserant,[†,‡] Gaëtan Wicht,[†] Ole F. Göbel,[§] Eva Bocek,[†] Gian-Luca Bona,[⊥,¶,#] Thomas Geiger,[†] Roland Hany,[†] Raffaele Mezzenga,[‡] Stefan Partel,[△] Peter Schmid,[□] Wolfhard Bernd Schweizer,[∥] and Jakob Heier[†,*]

[†]Laboratory for Functional Polymers, Empa, Swiss Federal Laboratories for Materials Testing and Research, CH-8600 Dübendorf, Switzerland, [‡]Department of Health Sciences & Technology, Laboratory of Food and Soft Materials Science, ETH Zürich, CH-8092 Zürich, Switzerland, [§]Bruker Nano GmbH, 76187 Karlsruhe, Germany, [⊥]Empa, Swiss Federal Laboratories for Materials Testing and Research, CH-8600 Dübendorf, Switzerland, [¶]Department of Information Technology and Electrical Engineering, ETH Zürich, CH-8092 Zürich, Switzerland, [#]Laboratory for Photonic Materials and Characterization, École Polytechnique Fédérale de Lausanne (EPFL), CH-1015 Lausanne, Switzerland, [△]Research Center for Microtechnology, Vorarlberg University of Applied Sciences, 6850 Dornbirn, Austria, [□]Laboratory for Analytical Chemistry, Empa, Swiss Federal Laboratories for Materials Testing and Research, CH-8600 Dübendorf, Switzerland, and [∥]Laboratory for Organic Chemistry, ETH Zürich, CH-8093 Zürich, Switzerland

ABSTRACT Studying and understanding the conditions under which organic semiconductors can be engineered to form aligned single crystals in thin films is of primary importance owing to their unique orientation-dependent optoelectronic properties. Efforts to reach this goal by self-assembly from solution-processed films have been rewarded only with limited success. In this article we present a new method to grow single crystalline thin films *via* solvent annealing. We identify solvate crystal growth in combination with a specific film dewetting morphology as key to successful fabrication of single crystals. Furthermore, these 2D single crystals can align on chemically patterned substrates to minimize their interfacial energy. We explore *in situ* the conditions for crystal formation and alignment.

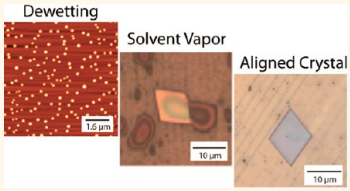

KEYWORDS: organic single crystal · cyanine dye · thin film · patterning · dewetting

The use of soluble organic semiconductors in electronic devices such as organic field effect transistors (oFETs), organic light emitting diodes, and organic solar cells is a prospering research field experiencing rapid advancements.[1−4] Competitive performances for oFETs though have been reported only for single crystalline vapor deposited materials[5,6] with few grain boundaries and a high molecular order.[7] While solution processable molecules can be deposited cheaply onto substrates by spin coating[8] or inkjet printing,[9] the obtained films are typically amorphous or polycrystalline due to the complex processes that take place on the molecular level during solvent evaporation. Often crystals can be grown by a postdeposition treatment from amorphous or polycrystalline thin films, such as annealing or solvent vapor annealing (SVA).[10] The presence of solvent molecules allows molecules to rearrange and adopt configurations closer to thermodynamic equilibrium than the metastable state obtained directly after spin coating.[11,12] The nature of the substrate plays a major role in crystal growth.[13] For example, recrystallization is supported by a thin condensed solvent layer on the substrate surface.[14,15] The growth of large single crystals during SVA is facilitated on polymer base films that are soluble in the solvent used.[16] SVA typically utilizes poor solvents for the material under consideration,[17] only a few reports discuss SVA with good solvents.[10] For example, large single crystals of a solvate crystal of [6,6]-phenyl-C61-butyric acid methyl ester (PCBM) with the solvent chlorobenzene could be grown.[18] Investigations into different crystal forms of the same molecule, such as solvate crystals, offer new opportunities in crystal design.[19] Applications are not limited to pharmaceuticals and agrochemicals, but extend to organic semiconductors like C60[20] and Alq3.[21] Lethal to large area single crystal growth is the presence of many randomly oriented nuclei. From this the strategy had emerged to control nucleation by using patterned substrates.

* Address correspondence to jakob.heier@empa.ch.

Received for review April 5, 2013 and accepted May 24, 2013.

Published online May 24, 2013
10.1021/nn401679s

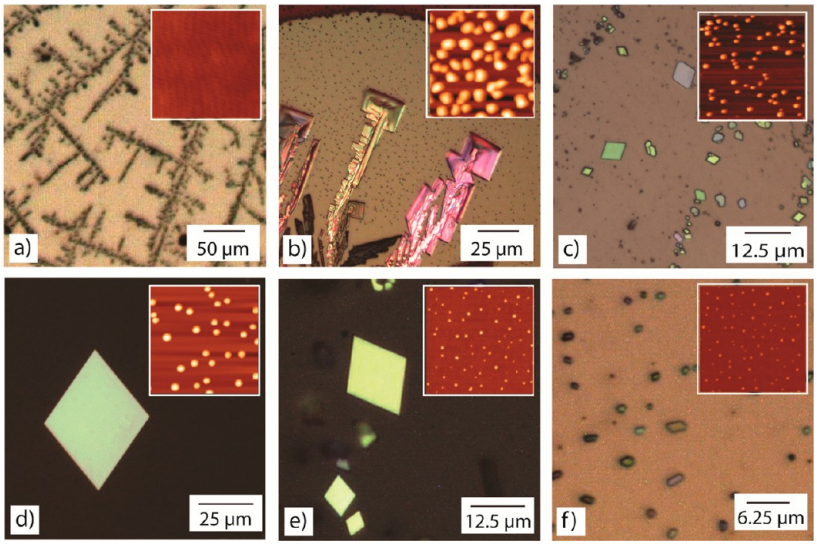

Figure 1. Cyanine crystals after solvent annealing in a saturated chlorobenzene atmosphere for 16 h. (a) Dendritic crystals grown from a continuous 300 nm thick CyC film on gold. (b) Sectored plate crystal and (c) single crystals grown from a dewetted CyC film on a gold surface. (d−f) CyC single-crystals grown from films dewetted from pure SAM substrates. SFM scans (5 μm × 5 μm) of the spin coated films before solvent annealing are shown in the insets.

Briseno *et al*. created a surface with printed octadecyltriethoxysilane (OTS) nucleation regions small enough to allow only one nucleation event.[22] Goto *et al*. designed a micropattern with small nucleation control areas and large crystal growth areas.[23]

Organic single crystals often show an anisotropic molecular arrangement, consequently, charge transport depends strongly on their orientation.[24] For the integration of single crystals into devices, the control of the orientation of the single crystal is thus of importance.[25] Up to now only a few practical approaches have been suggested for solution processed films. One method for enhanced in-plane orientation is the experiment of Goto mentioned before. Mascara *et al*. and Kumatani *et al*. grew needle-shaped single crystals of aluminum-tris(8-hydroxyquinolin) (Alq3) and dioctylbenzothienobenzo-thiophene (C8-BTBT) in patterned trenches by SVA, respectively.[26,27] In that case an artificial groove corrects the crystal orientation during growth. We here report a mechanism that allows for the growth of large single crystalline domains of a cyanine dye in thin films. The orientation of the crystals can be guided by growing crystals on a substrate with patterned self-assembled monolayers (SAM) manufactured by microcontact printing (μCP).[28] The crystal favors orientations that minimize the interfacial energy between crystal and substrate. Interest for cyanine single crystals arises from the extraordinary electro-optical properties of their aggregated state.[29,30] It is known that cyanine dyes which precipitate from solution primarily form solvate crystals.[31] In thin films, single crystals have been only grown epitaxially on lipid monolayers.[32]

RESULTS AND DISCUSSION

Single Crystal Formation. Key to single crystal growth lies in a particularity of the growth method: We start crystallization from a small number of nulcei present in amorphous islands that formed during film dewetting.[33] Crystallization itself proceeds in a second solvent annealing step. In chlorobenzene vapor, thin film single solvate crystals form. Figure 1 shows optical micrographs of different crystal morphologies of the cyanine dye 1,1′-diethyl-3,3,3′,3′-tetramethylcarbocyanine perchlorate (CyC) after solvent annealing. In the inset we show scanning force microscopy (SFM) scans of the films directly after spin coating. On a gold substrate (Figure 1a−c) and with decreasing solution concentration, the crystal morphology changes from dendritic to an ideal single crystal. The differences can be explained by the varying starting film morphologies, changing from continuous to individual dewetting droplets (insets to the Figure 1a−c). On a pure SAM (Figure 1d−f), decreasing the solution concentration leads to a decrease in dewetting droplet size. Here, always single crystals were observed, the smaller the dewetting droplets were , the smaller were the resulting crystal. This is already an interesting observation as such: different crystals can be grown solely by changing the boundary conditions while leaving the crystals growth conditions constant. Most commonly phase transformations in crystalline materials are the result of a change in the degree of supersaturation. In our approach the growth speed is regulated *via* the overall availability of molecules by changing the density of dewetting droplets. For growth at high rates, the growth front becomes unstable and a complex dendritic, ramified, or fractal pattern can be observed, whereas for sufficiently slow growth, the formation of ideal crystals becomes possible. The formation of the dewetting CyC droplet phase upon spin coating is described in detail in the Supporting Information.

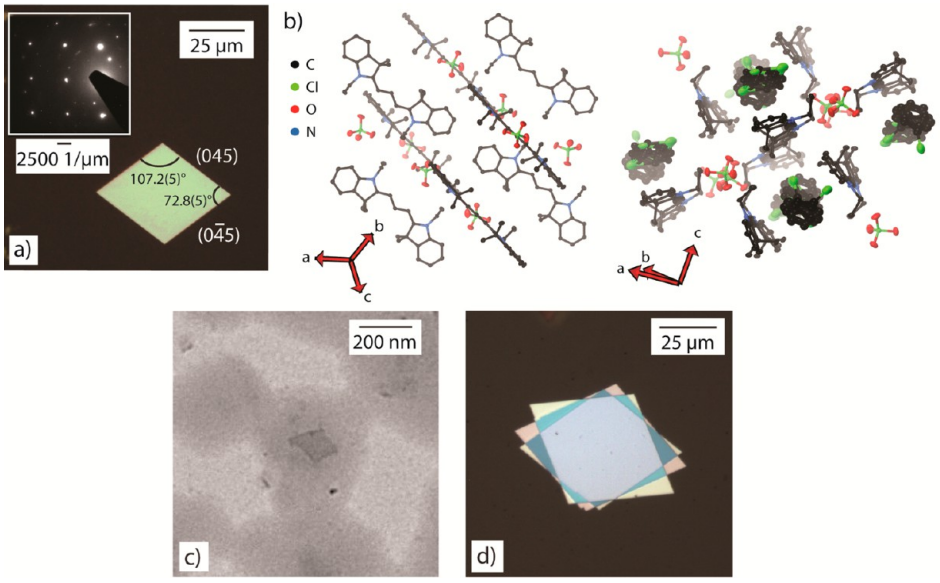

Figure 2. (a) Rhomb-shaped cyanine single crystal with the corresponding crystal planes. Inset: selected-area electron diffraction pattern of the rhomb-shaped crystal. (b left) Molecular packing of the crystal showing the layers formed by CyC and perchlorate counterions (chlorobenzene is omitted for clarity). (b right) Molecular packing of the crystal, the chlorobenzene solvent molecules lie in tubes formed by four CyC molecules, only two of the eight disordered sites of chlorobenzene are shown for clarity. Ellipsoids of the cyanine and perchlorate moieties are at the 50% level, hydrogen atoms are omitted for clarity. (c) TEM image of a crystal nucleus inside a droplet. (d) A stack of three single crystalline rhombi.

Single Crystal Structure Analysis. In all samples during early crystal growth, the most frequently observed crystal morphology was a rhombus with an acute angle of 72.8(5)° and an obtuse angle of 107.2(5)° (Figure 2a). A clear rhomb-shaped morphology can be noted at crystal sizes (length of the longer diagonal) of 5 μm. Rhomb-shaped crystals rarely grow larger than 40 μm, with heights ranging from 100 to 1000 nm. The crystal structure of the dye was determined by single crystal X-ray diffraction for crystals grown by vapor diffusion[34] with chlorobenzene as solvent and cyclohexane as antisolvent. The molecular packing of the crystal is shown in Figure 2b. The crystal is a solvate crystal of a cyanine dye,[35] for each dye chromophore we counted two chlorobenzene molecules. Gas chromatography–mass spectrometry (GC–MS) showed that the ratio of dye to solvent in the thin film crystal is the same as in the bulk crystal. This suggests that both types of crystals are of the same phase. The almost quadratic pattern of diffraction peaks (Figure 2a inset) strongly suggests that the (100) plane is oriented parallel to the substrate (b≈c). On the basis of the out-of-plane orientation, one can attempt to partially index the side faces of the rhomb-shaped crystals. We conclude that the crystals are most likely a combination of {100} and {h45} faces (Figure S2 in the Supporting Information).

Crystal Nucleation. Single crystals for further investigation were grown in the following 2 step process: first, a film consisting of amorphous dewetting droplets was manufactured by spin coating a CyC solution onto a gold surface with a SAM stripe pattern or a 2D pattern of 2 μm periodicity.

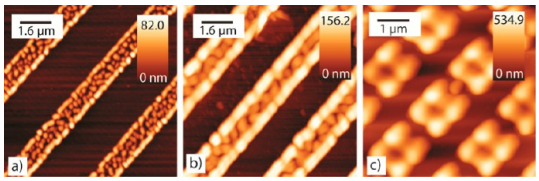

Figure 3. Cyanine film morphologies on patterned SAMs. Films were spin-cast from saturated isopropyl alcohol solutions at 1000 rpm (a) and 500 rpm (b) on a stripe pattern and drop-cast onto a 2D grating (c).

Liquids dewetting from a patterned surface have attracted much interest in the past decade as they have proven to be an easy route for patterning of organic materials from solutions.[36] A chemically heterogeneous substrate may drive substances to specific surface areas. A cyanine film coated from saturated isopropyl alcohol solution onto patterned SAMs will decompose into individual droplets populating only the gold surface (Figure 3). By utilizing a patterned SAM, the film can be destabilized into a much denser array of dewetting droplets compared to a film dewetting from a homogeneous substrate, and still single crystal growth is observed. The denser the droplet array, the larger the single crystals that can be grown. Later we will show that the patterned SAM also reorients the crystal during growth.

We here identified the spin-casting step as the crystal nucleation stage. An optical analysis of the morphology of the individual droplets directly after spin coating suggests that all droplets are amorphous. Only a TEM analysis of the as cast film shows that in a few droplets a nanocrystal had formed that may act as

nucleus for crystal growth. These crystals are about 200 nm in size and show already a rhomb-shaped morphology (Figure 2c). We can only speculate on the conditions that are necessary for the growth of these nuclei. By spin coating from saturated solutions, the connected solvent evaporation will bring the system immediately into a regime of supersaturation. These nuclei were not found in films that wet the surface, the process of dewetting is thus a necessary condition for crystal nucleation. Also the dendritic crystals grown from continuous films (Figure 1a) suggest only a few nucleation events in the wetting film. Furthermore, during crystal growth almost no additional nuclei were formed. Once we observed three layered single crystalline plates of different orientation, but with exactly the same size (Figure 2d). Here three nuclei were initially present in one dewetting droplet.

Crystal Growth. Crystal growth occurred in a second solvent annealing step. The early stage is characterized by solvent uptake by the amorphous cyanine domains; the first single crystals became visible in the optical microscope after about 20 min of solvent annealing. As chlorobenzene is a good solvent for the dye, we may assume that a significant number of solvent molecules are adsorbed and can diffuse into the dye domains and allow for solvent-mediated amorphous-to-crystalline transformations. We can estimate the solvent uptake necessary to lower the glass transition temperature of the dye to below room-temperature.[37] Using a melting temperature of T_{ms} = 228 K for chlorobenzene, and a glass transition temperature of the dye of T_g = 447 K, we found that the chlorobenzene volume fraction of the droplet should be at least 27%. This is a significant amount and explains the possibility of the dye molecules to rearrange within the bulk of a droplet. Solvent uptake also leads to coalescence of the initial droplet distribution as shown in Figure 3, to a distribution as shown in Figure 4 and Figure 5. The figures further show the morphological transformation of amorphous droplets into single crystals. Two growth modes could be distinguished: in the fast mode, the growing crystal is in direct contact with an amorphous cyanine droplet (Figure 4a). The optical images unequivocally show that the crystal grows at the cost of the merging dye droplet. We believe that the organization of exactly one dye molecule and two solvent molecules at the growth front limits the crystal growth rate. The key to single crystal growth is therefore the formation of a solvate crystal with the good solvent chlorobenzene. Figure 4b shows the growth kinetics of three individual crystals. The crystal shape is conserved at all times which implies that the growth rate is the same at all crystal faces. Otherwise the crystal would also change its shape. During growth, the height increased maximally by 10%. An Avrami analysis of the same data resulted in a growth exponent of 2, confirming a two-dimensional growth without nucleation.[38,39] In the

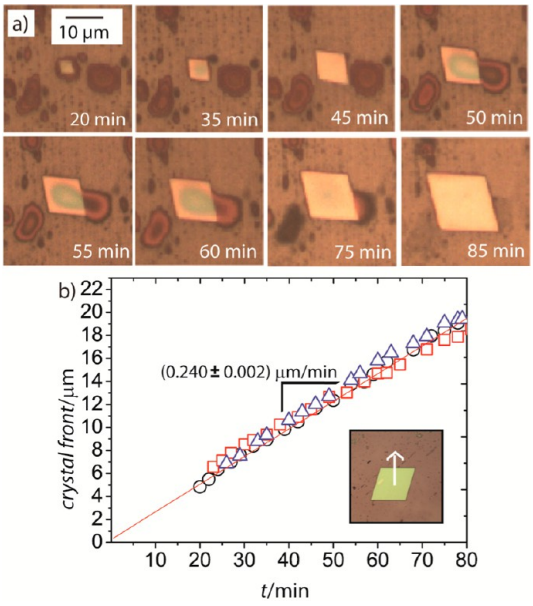

Figure 4. Single crystal growth when in contact with a liquid droplet (fast mode). (a) In-situ monitoring of the growth of a single crystal in contact with a droplet under an optical microscope. (b) Corresponding growth kinetics of three different crystals.

slow mode, crystal growth occurs *via* long-range transport of cyanine dyes to the crystal. Crystal growth is accompanied by the development of a droplet depletion zone around the growing crystal (Figure 5a). The rate measured for this mode is about 25 times slower than when the drops are in direct contact with the crystals (Figure 5b). We observed that over ca. 10 h the depleted surface varies linearly with time which allowed the calculation of an apparent diffusion coefficient of 1.3×10^{-10} m^2/s. This value has the same order of magnitude as the diffusion coefficient of dye molecules in solution, while a surface diffusion coefficient is orders of magnitudes lower.[40] As soon as the liquid droplet feeding an individual crystal is consumed, the growth mode switches from fast to slow. When the depletion zones of neighboring crystals overlap, crystal growth slows down and eventually comes to a stop. From Figure 5a we can also estimate the number of nucleation events. One crystal evolved out of an array of 200 droplets.

Crystal Orientation. A desired control over crystallization includes crystal orientation in the substrate plane. Here we show that the introduced chemical substrate pattern (gold/SAM stripe pattern with 2 μm periodicity) influences the crystal orientation. The angle φ between the long diagonal of the crystal and the line direction was measured for 307 crystals with two different size distributions. The group of smaller crystals has an average diagonal length of 10 μm, while the group of larger crystals has an average diagonal length of 19 μm. The larger crystals were manufactured from a denser droplet film; the solvent annealing time was

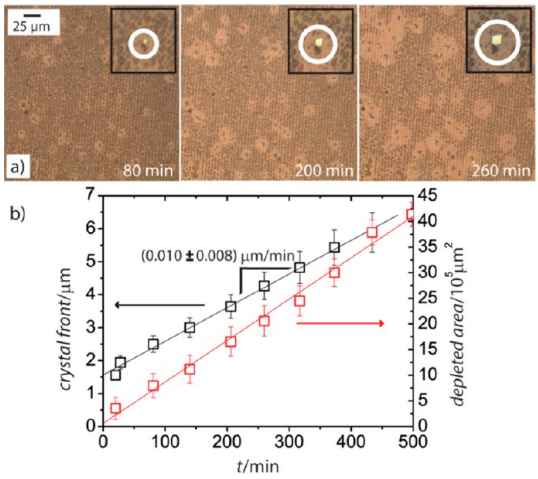

Figure 5. Surface-diffusion-controlled growth of a crystal (slow mode). (a) In-situ monitoring under an optical microscope. In the inset we show one crystal at higher magnification. The size of the insets is 35 μm × 35 μm. (b) Corresponding growth kinetics of one crystal and the area of the depleted region.

12 h in both cases. For the smaller crystals, preferential orientations of the rhombi with respect to the line direction were found at 0°, 8°, 36°, 53°, and 90° (Figure 6a center). It is conspicuous that most of these orientations correspond to geometries where either a diagonal or a side line of the rhombus is parallel to the substrate pattern. For comparison, the random angle distribution of rhombi on a nonstructured surface is shown in Figure 6a top. The larger crystals show a different and less pronounced angle distribution due to the wider size distribution (Figure 6a bottom). We recall that during growth, all four crystal faces perpendicular to the substrate advance at the same rate. From here we can rule out that the crystal appears to change its orientation because of anisotropic feeding of the crystals. One must thus assume that either the nuclei have a preferred orientation, or the crystals as a whole are capable of moving and rotating with respect to the substrate. While we cannot rule out a prearrangement of the nuclei, the latter was observed directly: the inset of Figure 6b is an overlay of the images of a rhomb-shaped single crystal shown in Figure 6a at times $t = 20$, 50, and 85 min. We observe a rotational as well as a lateral movement of the growing crystal while in contact with the liquid droplet. The overall rotational motion of one crystal with time is shown in Figure 6b. The change in angle over the measurement time is larger than 10° and carries out an oscillating movement. Such a motion of the entire crystal is only possible when the friction between crystal and substrate is smaller than the driving force for displacement. A closer look at the microscopic images reveals that the crystal is not in direct contact with the patterned SAM, but floats on a thin solvent layer which wets the crystal surface. In the best case of hydrodynamic lubrication, for the crystal to move only the friction resulting from the viscosity of the solvent has to be overcome.[41] Assuming a wetting layer thickness of $d = 100$ nm, the energy dissipated by friction when moving a crystal of size $A = 25\ \mu m^2$ with a velocity of $v = 5 \times 10^{-9}$ m/s by $\Delta x = 1\ \mu$m can be estimated by

$$\Delta G_f = \frac{\eta A v \Delta x}{d}$$

whereby $\eta = 0.75$ mPa·s is the bulk viscosity of chlorobenzene. The velocity has been estimated from optical microscope images. We obtain a value of $\Delta G_f \approx 10^{-21}$ J. We expect that for liquid layer thicknesses down to molecular dimensions the response is still liquid-like, but with a viscosity increased by orders of magnitude.[42] The driving force for this motion is the minimization of the overall interaction energies between crystal, lubrication solvent, and substrate. Depending on the solvent layer thickness, the interaction energies comprise surface energies and van der Waals forces (disjoining pressures).[43] Practically, a most favored position on the stripes will reposition the crystal such that the contact area of the crystal with the SAM stripes decreases. We calculate the energy gain when shifting the model crystal from the calculation above over a SAM stripe pattern of 2 μm periodicity from an energetically most unfavorable to a most favorable position, assuming an effective surface tension difference of 10 mN/m between the gold and the SAM surface. The energy gain then amounts to $\Delta G_{int} = 5 \times 10^{-14}$ J, orders of magnitudes higher than the dissipation of energy by frictional forces calculated before. In the real system the frictional forces are most likely much higher, but the values confirm that the mechanism is feasible. To further explain the experimental data we calculated effective interfacial energies of a rhomb-shaped crystal on a stripe pattern of 2 μm periodicity as function of position and angle φ for four different crystal sizes (see Experimental Methods, Figure 6c). The interfacial energies show distinguishable minima and maxima, their positions, and more pronounced, their amplitudes change with crystal size. The strong variation in interfacial energy with lateral motion perpendicular to the stripe pattern for crystals covering an odd number of stripes (e.g., 11.7 and 15 μm) reflects the following: at the energy maximum, the crystal covers three and four gold stripes, but extends over four and five SAM stripes, respectively. At the energy minima, this situation is reversed. For cases where the crystal covers an even number of stripes (e.g., 10.0 and 13.4 μm), any motion of the crystal has a minor effect on the overall interfacial energy. Under crystal width we here understand the length of the side faces. For each crystal size, a certain position and orientation minimizes the interfacial energy (represented by Figure 6c). We thus must assume that during growth the crystal will continuously adapt angle and position to the applicable energy minimum, such a motion is

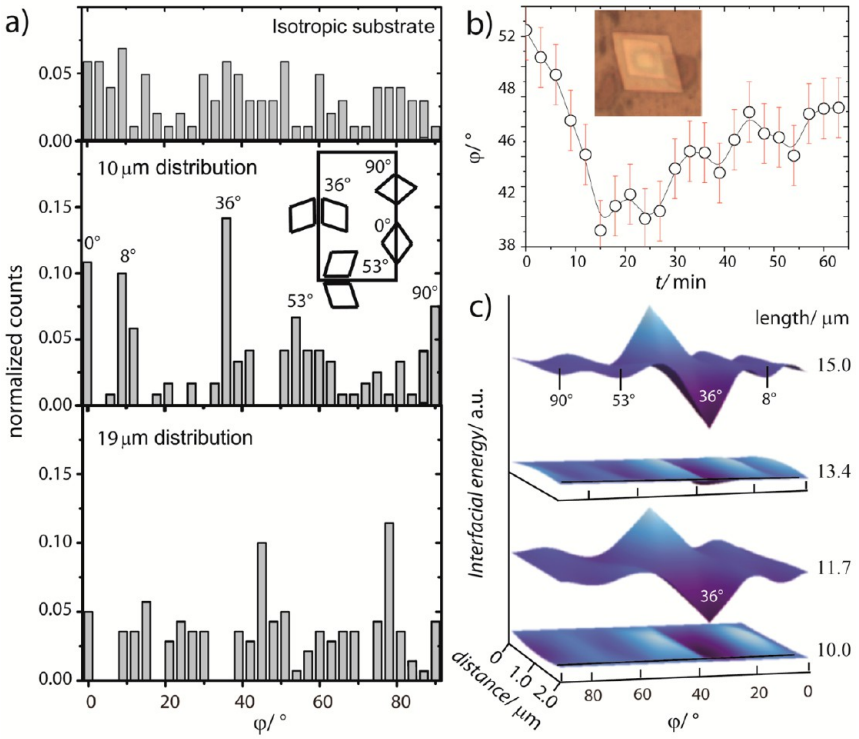

Figure 6. Oriented crystallization. (a) Angular distribution of the orientation of single crystals on a homogeneous substrate (top) and on a SAM line pattern with 2 μm periodicity. The middle and bottom histograms show the distribution for crystals of different sizes. Preferred orientations are noticeable on the patterned substrates. Inset: corresponding crystal orientations. (b) Rotational movement of a single crystal in contact with a liquid droplet with time. (c) Calculation of the interfacial energy as a function of φ for $0° \leq \varphi \leq 90°$ and a lateral movement perpendicular to the stripe pattern of one periodicity for 15.0, 13.4, 11.7, and 10.0 μm large crystals.

indeed observed experimentally (Figure 6b). The minimum found at 36° is especially pronounced and returns periodically during crystal growth to that position (Figure 6c). Practically, a growing crystal oriented between 26° and 46° to the pattern will repeatedly experience a force that will orient the crystal to 36°. Also other well-defined minima in the interfacial energy plot coincide with the statistically observed orientations of the 10 μm crystal size distribution.

To improve the alignment, we attempted to better match substrate pattern and crystal geometry. A hexagon has angles of 60° and 120°, being closer to the angles of the rhomb shaped crystal. In most cases the dewetting droplet is pinned to the SAM pattern (Figure 7a). From our data it is hard to evaluate what the influence of this contact line pinning on crystal orientation is. On a hexagonal SAM pattern, coalescing dye droplets often take the shape of a rhombus (Figure 7b) and evolve into a perfectly aligned crystal (Figure 7c). Nevertheless, the rhombus is not the only shape that evolves during coalescence, and we suspect that other shapes prevent crystal alignment. We may further improve the alignment statistics with a droplet pattern with the exact angles of the crystal, but it seems that here contact line pinning has a stronger influence than the interfacial energy minimization.

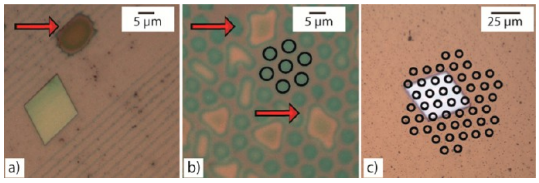

Figure 7. Crystal orientation on a hexagonal pattern. (a) Contact line pinning of a coalescence droplet on a 1D pattern. (b) Coalescence on a hexagonal pattern results in droplets, rods (from 2 droplets), triangles (3 droplets), and rhombs (4 droplets) with angles close to that of the crystals. (c) These patterns yield well aligned rhomb-shaped crystals.

CONCLUSIONS

In summary, we introduced a new method to grow single solvate crystals in thin films by solvent annealing. The crystal growth method should be applicable to the large class of molecules that can form solvate crystals. Most likely by far not all crystal forms of organic molecules have been discovered. The nature of the dewetting pattern of the starting film allows controlling crystal growth, especially the growth direction of the crystals can be controlled with patterned SAMs. A model based on the minimization of interfacial energy can convincingly predict the favored positions on the surface. The design of a substrate pattern for crystal orientation is rather complicated and needs to

not only take the specific shape of the crystal into account. A proper design of the starting dewetting morphology may allow full control over crystal orientations and positions by self-assembly and may open low cost fabrication routes for efficient organic electronic devices.

EXPERIMENTAL METHODS

Preparation of Patterned Substrates. Patterned self-assembled monolayers (SAMs) were prepared by microcontact printing (μCP).[28] Materials for the deposition were purchased from Cerac, Inc. A 3 nm thick chromium adhesion layer and a 10 nm thick gold layer were deposited at a typical deposition rate of 0.1 Å/s at a pressure of 6×10^{-6} mbar onto microscope glass slides. The patterned poly(dimethylsiloxane) stamp (PDMS) was prepared by pouring a vacuum-degazed 10:1 (wt) base:curing-agent mixture (Sylgard 184, Dow Corning) on a patterned silicon wafer bearing 280 nm-deep patterns with different periodicities. This mixture was cured at room temperature for 24 h. The patterned PDMS stamp was swelled for 5 s by drop contact with a 0.5 mM solution of octadecanethiol (Sigma Aldrich) and dried under nitrogen flow for 10 s. It was then maintained in contact with a freshly deposited gold surface for 10 s, resulting in a stripe pattern of CH3-terminated SAMs (hydrophobic) on the gold surface.

Film Formation. The cyanine dye 1,1′-diethyl-3,3,3′,3′-tetramethylcarbocyanine perchlorate (CyC) was synthesized in our laboratory.[44,45] CyC was dissolved in isopropyl alcohol at different concentrations and then spin-cast onto patterned gold substrates. Thicknesses were adjusted by varying the concentration or the spin speed. Consecutively the films were solvent-annealed in a saturated chlorobenzene atmosphere in a self-built chamber allowing *in situ* optical monitoring. Solvents were purchased from Aldrich and used as received.

Characterization. Scanning probe microscopy surface scans of the samples were performed with a Nanosurf Mobile S (Nanosurf AG, Liestal, Switzerland) in tapping mode at a resonance frequency of 170 kHz with silicon cantilevers from Mikromasch, Nanosensors TM.

Transmission electron microscopy (TEM) was performed with a Philips CM 30 at an operating voltage of 300 kV. Samples were prepared on amorphous carbon coated TEM grids from Agar Scientific.

Single-crystal X-ray analysis of the cyanine dye was performed using a Bruker Nonius APEX-II CCD diffractometer with MoKα radiation (λ = 0.71073 Å) and graphite monochromator. The structure was solved by direct methods (SHELXS97) and refined by full-matrix least-squares on F2 (SHELXL97).[46] Non-hydrogen atoms with the exception of the disordered chlorobenzene were refined anisotropically, H-positions were calculated and included in the structure factor calculation. Dye: C27H33N2+, ClO4-, C6H5Cl, MW = 597.55, space group monoclinic *C*2/*c*, cell a = 23.9162(7) Å, b = 16.8152(6) Å, c = 15.6580(6) Å, β = 92.811(1)°, z = 8, z' = 1, *R*-factor = 7.33% (378 parameters, 5130 $I > 2\sigma(I)$). Crystallographic data (excluding structure factors) for the structure(s) reported in this paper have been deposited with the Cambridge Crystallographic Data Centre as supplementary publication no. CCDC-923770.

Gas chromatography−high resolution mass spectrometry (GC-HRMS): quantitative determination of chlorobenzene was carried out on a MAT 95 mass spectrometer (Thermo Finnigan MAT, Bremen, Germany) coupled to a gas chromatograph HRGC Mega 2 series (Fisons Instruments, Rodano, Italy). GC separation was effected on a 20 m × 0.30 mm glass capillary coated column with a DB-5 analogue stationary phase (PS 086, Fluka, Buchs, Switzerland) with a film thickness of 2.4 μm using hydrogen at 40 kPa as carrier gas. The following temperature program was used: 40 °C (1 min), 5 °C/min up to 150 °C. The mass spectrometer was operated in high resolution mode (mass resolution $m/\Delta m$ = 7800) using electron ionization (electron energy 70 eV) at an ion source temperature of 180 °C. Chlorobenzene was detected by selected ion monitoring (SIM) of the molecular ions at m/z 112.0074 (C6H535Cl+) and 114.0045 (C6H537Cl+). Quantification was based on an ethanolic solution containing 500 ppb (v/v) chlorobenzene as an external standard and evaluation of the signal areas of the mass chromatograms. For this experiment, fully crystallized films were dissolved in ethanol. The chlorobenzene concentration value obtained by this method was compared to the concentration of cyanine present in the same solution measured by UV−vis. A ratio of 1.90 ± 0.2 was found between solvent and dye in the crystals.

Interfacial Energy Calculation. Minimization of the interfacial energy between the rhomb-shaped crystals and the patterned substrates was computed on Mathematica. The size and orientation of the rhombi was varied above a fixed patterned geometry using a 2D rotation matrix and the corresponding energy was computed by a sum of integrals on the successive covered gold/SAM stripes. For the calculations we chose an arbitrary value for the energy difference between the crystal covering the gold or SAM surface as it does not change the qualitative picture. The surface energies of an amorphous CyC film have been measured before (γ = 34.3 mN/m),[47] while the surface energy of the crystal is unknown. The surface energy value for a pure CH_3-terminated SAM on Au is γ = 19−20 mN/m.[48] The initial surface energy of neat (111) Au can be as high as γ = 1250 mN/m,[49] but this value decreases rapidly when the surface is exposed to air.[50] As a low estimate for an effective interfacial tension difference between the (crystal-solvent-gold) and (crystal-solvent-SAM) interface we chose a value of γ = 10 mN/m.

Conflict of Interest: The authors declare no competing financial interest.

Acknowledgment. This work is supported by the Swiss National Science Foundation (SNF) under Grant No. 200021_132502. We acknowledge U. Müller and the Swiss Scanning Probe Microscopy User Laboratory at Empa for SPM support. We thank S. Handschin (ETH) for designing the solvent vapor annealing chamber. We thank F. Nüesch and M. Heuberger (Empa) for helpful discussions.

Supporting Information Available: Studies on dewetting, single crystal morphology, and indexing of faces. This material is available free of charge *via* the Internet at http://pubs.acs.org.

REFERENCES AND NOTES

1. Forrest, S. R. The Path to Ubiquitous and Low-Cost Organic Electronic Appliances on Plastic. *Nature* **2004**, *428*, 911–918.
2. Sirringhaus, H. Device Physics of Solution-Processed Organic Field-Effect Transistors. *Adv. Mater.* **2005**, *17*, 2411–2425.
3. Xiao, L.; Chen, Z.; Qu, B.; Lu, J.; Kong, S.; Gong, Q.; Kido, J. Recent Progresses on Materials for Electrophosphorescent Organic Light-Emitting Devices. *Adv. Mater.* **2011**, *23*, 926–952.
4. Brabec, C. J.; Durrant, J. R. Solution-Processed Organic Solar Cells. *MRS Bull.* **2008**, *33*, 670–675.
5. Virkar, A. A.; Mannsfeld, S.; Bao, Z.; Stingelin, N. Organic Semiconductor Growth and Morphology Considerations for Organic Thin-Film Transistors. *Adv. Mater.* **2010**, *22*, 3857–3875.
6. Gershenson, M. E.; Podzorov, V.; Morpurgo, A. F. Colloqium: Electronic Transport in Single-Crystal Organic Transistors. *Rev. Mod. Phys.* **2006**, *78*, 973–989.
7. Sundar, V. C.; Zaumseil, J.; Podzorov, V.; Menard, E.; Willett, R. L.; Someya, T.; Gershenson, M. E.; Rogers, J. A. Elastomeric Transistor Stamps: Reversible Probing of Charge Transport in Organic Crystals. *Science* **2004**, *303*, 1644–1646.
8. Meyerhofer, D. Characteristics of Resist Films Produced by Spinning. *J. Appl. Phys.* **1978**, *49*, 3993–3997.

9. Sirringhaus, H.; Kawase, T.; Friend, R. H.; Shimoda, T.; Inbasekaran, M.; Wu, W.; Woo, E. P. High-Resolution Inkjet Printing of All-Polymer Transistor Circuits. *Science* **2000**, *290*, 2123–2126.
10. Toffolo, F.; Brinkmann, M.; Greco, O.; Biscarini, F.; Taliani, C.; Gomes, H. L.; Aiello, I.; Ghedini, M. Influence of the Metal Center on the Morphology of Coordination Compounds Thin Films. *Synth. Met.* **1999**, *101*, 140–141.
11. Gregg, B. A. Evolution of Photophysical and Photovoltaic Properties of Perylene Bis(phenethylimide) Films Upon Solvent Vapor Annealing. *J. Phys. Chem.* **1996**, *100*, 852–859.
12. Brinkmann, M.; Wittmann, J. C.; Chaumont, C.; Andre, J. J. Effects of Solvent on the Morphology and Crystalline Structure of Lithium Phthalocyanine Thin Films and Powders. *Thin Solid Films* **1997**, *292*, 192–203.
13. Pratontep, S.; Nüesch, F.; Zuppiroli, L.; Brinkmann, M. Comparison Between Nucleation of Pentacene Monolayer Islands on Polymeric and Inorganic Substrates. *Phys. Rev. B* **2005**, *72*, 085211–085215.
14. Datar, A.; Oitker, R.; Zang, L. Surface-Assisted One-Dimensional Self-Assembly of a Perylene Based Semiconductor Molecule. *Chem. Commun. (Cambridge, U. K.)* **2006**, *15*, 1649–1651.
15. Treossi, E.; Liscio, A.; Feng, X.; Palermo, V.; Müllen, K.; Samorì, P. Temperature-Enhanced Solvent Vapor Annealing of a C_3 Symmetric Hexa-*peri*-Hexabenzocoronene: Controlling the Self-Assembly from Nano- to Macroscale. *Small* **2009**, *5*, 112–119.
16. Liu, C.; Minari, T.; Li, Y.; Kumatani, A.; Lee, M. V.; Pan, S. H. A.; Takimiya, K.; Tsukagoshi, K. Direct Formation of Organic Semiconducting Single Crystals by Solvent Vapor Annealing on a Polymer Base Film. *J. Mater. Chem.* **2012**, *22*, 8462–8469.
17. Vogelsang, J.; Lupton, J. M. Solvent Vapor Annealing of Single Conjugated Polymer Chains: Building Organic Optoelectronic Materials from the Bottom Up. *J. Phys. Chem. Lett.* **2012**, *3*, 1503–1513.
18. Colle, R.; Grosso, G.; Ronzani, A.; Gazzano, M.; Palermo, V. Anisotropic Molecular Packing of Soluble C60 Fullerenes in Hexagonal Nanocrystals Obtained by Solvent Vapor Annealing. *Carbon* **2012**, *50*, 1332–1337.
19. Braga, D.; Grepioni, F.; Maini, L. The Growing World of Crystal Forms. *Chem. Commun. (Cambridge, U. K.)* **2010**, *46*, 6232–6242.
20. Wang, L.; Liu, B.; Liu, D.; Yao, M.; Hou, Y.; Yu, S.; Cui, T.; Li, D.; Zou, G.; Iwasiewicz, A.; *et al.* Synthesis of Thin, Rectangular C_{60} Nanorods Using *m*-Xylene as a Shape Controller. *Adv. Mater.* **2006**, *18*, 1883–1888.
21. Muccini, M.; Brinkmann, M.; Gadret, G.; Taliani, C.; Masciocchi, N.; Sironi, A. Optical Spectroscopy of Unsolvated and Solvated Crystalline Alq_3. *Synth. Met.* **2001**, *122*, 31–35.
22. Briseno, A. L.; Mannsfeld, S. C. B.; Ling, M. M.; Liu, S.; Tseng, R. J.; Reese, C.; Roberts, M. E.; Yang, Y.; Wudl, F.; Bao, Z. Patterning Organic Single-Crystal Transistor Arrays. *Nature* **2006**, *444*, 913–917.
23. Goto, O.; Tomiya, S.; Murakami, Y.; Shinozaki, A.; Toda, A.; Kasahara, J.; Hobara, D. Organic Single-Crystal Arrays from Solution-Phase Growth Using Micropattern with Nucleation Control Region. *Adv. Mater.* **2012**, *24*, 1117–1122.
24. De Boer, R. W. I.; Gershenson, M. E.; Morpurgo, A. F.; Podzorov, V. Organic Single-Crystal Field-Effect Transistors. *Phys. Status Solidi A* **2004**, *201*, 1302–1331.
25. Liu, S.; Wang, W. M.; Briseno, A. L.; Mannsfeld, S. C. B.; Bao, Z. Controlled Deposition of Crystalline Organic Semiconductors for Field-Effect-Transistor Applications. *Adv. Mater.* **2009**, *21*, 1217–1232.
26. Mascaro, D. J.; Thompson, M. E.; Smith, H. I.; Bulovic, V. Forming Oriented Organic Crystals From Amorphous Thin Films on Patterned Substrates *via* Solvent-Vapor Annealing. *Org. Electron.* **2005**, *6*, 211–220.
27. Kumatani, A.; Liu, C.; Li, Y.; Darmawan, P.; Takimiya, K.; Minari, T.; Tsukagoshi, K. Solution-Processed, Self-Organized Organic Single Crystal Arrays With Controlled Crystal Orientation. *Sci. Rep.* **2012**, *2*, 1–6.
28. Kumar, A.; Whitesides, G. M. Features of Gold Having Micrometer to Centimeter Dimensions Can Be Formed through a Combination of Stamping with an Elastomeric Stamp and an Alkanethiol Ink followed by Chemical Etching. *Appl. Phys. Lett.* **1993**, *63*, 2002–2004.
29. Kobayashi, T.; Du, J.; Kida, Y. Ultrafast Real-Time Vibrational Dynamics in J-Aggregates. In *J-Aggregates*; Kobayashi, T., Ed.; World Scientific: Singapore, 2012; Vol. 2, pp 1–47.
30. Bradley, M. S.; Tischler, J. R.; Bulović, V. Layer-by-Layer J-Aggregate Thin Films with a Peak Absorption Constant of 10^6 cm^{-1}. *Adv. Mater.* **2005**, *17*, 1881–1890.
31. Dammeier, B.; Hoppe, W. Die Kristall- und Molekülstruktur von *N,N'*-Diäthyl-pseudoisocyaninchlorid. *Acta Crystallogr., Sect. B* **1971**, *B27*, 2364–2370.
32. Kirstein, S.; Möhwald, H. Structure and Optical Properties of a Monolayer Single Crystal of a Cyanine Dye. *Chem. Phys. Lett.* **1992**, *189*, 408–413.
33. Hashimoto, Y.; Karthaus, O. Preparation of an Ordered Array of Cyanine Complex Microdomes by a Simple Dewetting Method. *J. Colloid Interface Sci.* **2007**, *311*, 289–295.
34. Spingler, B.; Schnidrig, S.; Todorova, T.; Wild, F. Some Thoughts about the Single Crystal Growth of Small Molecules. *CrystEngComm.* **2012**, *14*, 751–757.
35. Wheatley, P. J. The Crystallography of Some Cyanine Dyes. Part II. The Molecular and Crystal Structure of the Ethanol Solvate of 3,3′-Diethylthiacarbocyanine Bromide. *J. Chem. Soc.* **1959**, 4096–4100.
36. Xue, L.; Han, Y. Pattern Formation by Dewetting of Polymer Thin Film. *Prog. Polym. Sci.* **2011**, *36*, 269–293.
37. Bicerano, J. Transition and Relaxation Temperatures. In *Prediction of Polymer Properties*; Hudgin, D. E., Ed.; Marcel Dekker, Inc.: New York, 1996; pp 169–262.
38. Avrami, M. Kinetics of Phase Change. *J. Chem. Phys.* **1939**, *7*, 1103–1112.
39. Menczel, J. D.; Judovits, L.; Prime, R. B.; Bair, H. E.; Reading, M.; Wier, S. Differential Scanning Calorimetry. In *Thermal Analysis of Polymers*; Menczel, J. D., Prime, R. B., Eds.; Wiley: New York, 2009; pp 58–114.
40. Inglesby, M. K.; Zeronian, S. H. Diffusion Coefficients for Direct Dyes in Aqueous and Polar Aprotic Solvents by NMR Pulsed-Field Gradient Technique. *Dyes Pigm.* **2001**, *50*, 3–11.
41. Myers, D. Friction, Lubrication and Wear. In *Surfaces, Interface and Colloids*; Wiley: New York, 1999; pp 456–460.
42. Granick, S. Motions and Relaxations of Confined Liquids. *Science* **1991**, *253*, 1374–1379.
43. Myers, D. Attractive Forces. In *Surfaces, Interface and Colloids*; Wiley: New York, 1999; pp 40–78.
44. Ernst, L. A.; Gupta, R. K.; Mujumdar, R. B.; Waggoner, A. S. Cyanine Dye Labelling Reagents for Sulforhydryl-Groups. *Cytometry* **1989**, *10*, 3–10.
45. Wang, J.; Cao, W.-F.; Su, J.-H.; Tian, H.; Huang, Y.-H.; Sun, Z.-R. Synthesis and Nonlinear Absorption of Novel Unsymmetrical Cyanines. *Dyes Pigm.* **2003**, *57*, 171–179.
46. Sheldrick, G. M. A Short History of SHELX. *Acta Crystallogr., Sect. A* **2008**, *64*, 112–122.
47. Heier, J.; Groenewold, J.; Huber, S.; Nüesch, F.; Hany, R. Nanoscale Structuring of Semiconducting Molecular Blend Films in the Presence of Mobile Counterions. *Langmuir* **2008**, *24*, 7316–7322.
48. Genzer, J.; Kramer, E. J. Wetting of Substrates with Phase-Separated Binary Polymer Mixtures. *Phys. Rev. Lett.* **1997**, *78*, 4946–4949.
49. Needs, R. J.; Mansfield, M. Calculations of the Surface Stress Tensor and Surface Energy of the (111) Surfaces of Iridium, Platinum and Gold. *J. Phys.: Condens. Matter* **1989**, *1*, 7555–7563.
50. Bartell, F. E.; Smith, J. T. Alterations of Surface Properties of Gold and Silver as Indicated by Contact Angle Measurements. *J. Phys. Chem.* **1953**, *57*, 165–171.